2010
2011

FACULTY OF SCIENCES

Master of Statistics: Epidemiology & Public Health Methodology

Masterproef

Statistical analysis of the spatial symmetry of periodic vegetation patterns in semi-arid lands

Promotor :
Prof. dr. Christel FAES

Promotor :
Prof. OLIVIER LEJEUNE

Vicky Dupont

Master Thesis nominated to obtain the degree of Master of Statistics , specialization Epidemiology & Public Health Methodology

Maastricht University

universiteit hasselt
UNIVERSITEIT VAN DE TOEKOMST

Universiteit Hasselt | Campus Diepenbeek | Agoralaan Gebouw D | BE-3590 Diepenbeek
Universiteit Hasselt | Campus Hasselt | Martelarenlaan 42 | BE-3500 Hasselt

2010
2011

FACULTY OF SCIENCES

Master of Statistics: Epidemiology & Public Health Methodology

Masterproef

Statistical analysis of the spatial symmetry of periodic vegetation patterns in semi-arid lands

Promotor :
Prof. dr. Christel FAES

Promotor :
Prof. OLIVIER LEJEUNE

Vicky Dupont

Master Thesis nominated to obtain the degree of Master of Statistics , specialization Epidemiology & Public Health Methodology

Maastricht University

universiteit hasselt
UNIVERSITEIT VAN DE TOEKOMST

Abstract

This master thesis was written in light of the ongoing research that is concerned with the existence and expanse of spatially periodic distributions of plants in arid and semi-arid areas. Since the availability of aerial photographs in the 1940s, many biological models have been developed to try to explain the spatial arrangement of these periodic vegetation patterns. Recent models predict the following sequence of patterns for increasing aridity: gaps of bare ground in a dense vegetation cover, alternating stripes of vegetation and bare ground, and spots of vegetation surrounded by bare ground. Most interestingly, these models predict a hexagonal symmetry in these gapped and spotted patterns. This statement has been investigated through the use of spatial statistics. In addition to the near-hexagonal symmetry hypothesis, other near-regular symmetries were also investigated (rhomboidal, square and triangular). The statistical analysis was performed on a gapped vegetation pattern in Kenya. The Complete Spatial Randomness hypothesis was rejected in favour of the regularity alternative. Of the investigated nearly regular point process models, the rhomboidal with angle 52° was the most likely point process to describe the spatial structure in the observed data.

Keywords: Complete Spatial Randomness; Hexagonal symmetry; Nearly regular point process; Spatial point pattern.

Foreword

This thesis is the end result of a 2-year master programme in Statistics at the University of Hasselt. The obtained end result would not have been possible without the help and support of some people. Therefore, I would like to use this foreword to express my gratitude to them. First, I would like to thank my supervisor at UHasselt, Christel Faes for her guidance and suggestions in writing the thesis and for her ideas in approaching the different challenges I came across when working on the thesis. I want to thank, Olivier Lejeune for all the input and thoughts about the subject and his everlasting positive energy and motivation. And I would also like to thank Vincent Deblauwe for providing all practical information on examples and data of the periodic vegetation patterns.
Finally, I would like to thank my parents and my beloved partner for their constant support and patience during the time I studied.

Vicky Dupont
September 12, 2011
Diepenbeek

Contents

Chapter 1

Introduction

This master thesis deals with a scientific problem in the field of ecology and biogeography. More specifically, this research is concerned with the existence and expanse of spatially periodic distributions of plants in arid and semi-arid areas. The statistical analysis of these periodic vegetation patterns relates to the subdiscipline of spatial statistics. This section gives a thorough introduction on the background and motivation of the research. The goal of the thesis is put forward as well as the proposed approach to the scientific problem. Finally, the outline of the structure of this thesis is provided.

1.1 Background and motivation of the research

Since the availability of aerial photographs in the early 1940s, many amazingly regular patterns in the vegetation of arid and semi-arid areas have been revealed all over the world. These vegetation patterns typically have wavelengths ranging from tens to hundreds of metres and can spread over extensive areas (up to several square kilometres), making them undetectable at ground level. Macfadyen (1950a,b) was the first to describe this phenomenon in British Somaliland. Since then vegetation patterns have been reported in several arid and semi-arid regions of the African, American and Australian continents. These regions are characterised by climates where the potential evapotranspiration substantially exceeds the mean annual precipitation.

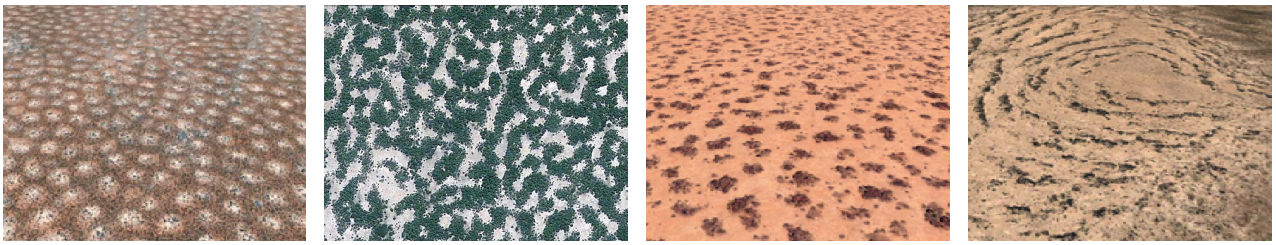

(a) Gaps of bare soil (b) Labyrinth stripes (c) Spots of vegetation (d) Tiger bush

Figure 1.1: Periodic vegetation patterns.

The first discovered patterns were made up of stripes of vegetation alternating periodically with sparsely vegetated areas or even bare ground. They were typically found on gently sloped terrains with a dominant orientation, generally perpendicular to the ground slope. By the resemblance of a tiger's coat markings, these patterns were named *tiger bush* (Clos-Arceduc, 1956). General theory

for these spatially periodic patterns is provided by self-organisation theory. Early explanations were based on water redistribution from bare areas to vegetated stripes through run-off (Thiéry et al., 1995; Klausmeier, 1999). However, these explanations postulate that anisotropy caused by the ground slope is necessary for pattern formation and were unable to explain the latter discovered spotted patterns which occurred on flat terrains. Other more recent models, that are also based on the movement of water, have been developed by Rietkerk et al. (2002); Meron et al. (2004). The occurrence of banded patterns in the immediate vicinity of spots established the need for a unified understanding of this patterning phenomenon. A recent explanation by Lefever & Lejeune (1997); Lefever et al. (2009) seems to progress towards this unified framework. They pose that pattern formation is based on plant-plant interactions. This thinking originates from the observation that the vegetation patterns are not specific to a particular kind of vegetation or soil. Regular patterns arise from an interplay between short-range facilitative interactions and long-range inhibitory interactions between plants. These interactions are supposed to be mediated by limiting resources, more specifically water. In isotropic environments, these models predict a sequence of spatially periodic patterns which are for increasing aridity: gaps of bare soil (Fig. 1.1(a)) in a dense vegetation cover , alternating stripes of vegetation and bare soil with no dominant orientation, i.e. labyrinths (Fig. 1.1(b)), and spots of vegetation (Fig. 1.1(c)) that finally ends in a desert. These models also predict that anisotropic factors, such as a ground slope lead to a shift from the aforementioned patterns towards stripes with a dominant orientation (tiger bush) (Fig. 1.1(d)). Figure 1.2 shows the predicted sequence of patterns for increasing aridity level and increasing ground slope. The vegetation density is represented by grey scale levels (dark: high density, light: low density).

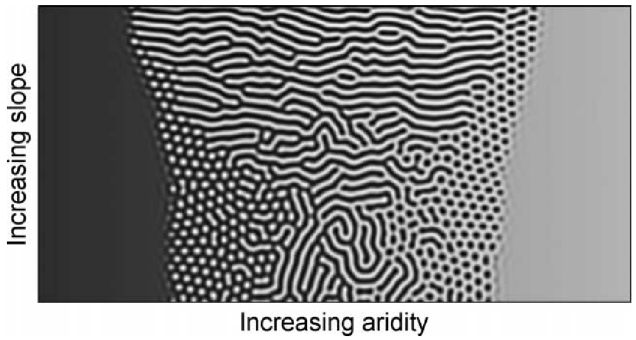

Figure 1.2: Continuous prediction of models for increasing aridity and ground slope (Deblauwe et al., 2011).

A special feature of these models is that they predict spots and gaps arranged in a hexagonal lattice. However, this hexagonal symmetry is rarely detected in the field and observed vegetation patterns are expected to be far from this asymptotic structure. Possible reasons could be that environmental anisotropies related to the soil, vegetation or climate have destabilised the hexagonal structure or that not enough time has passed to allow for the emergence of a clear hexagonal symmetry. In this setting, questions arise whether observed vegetation patterns (spots or gaps) actually tend towards a structure of hexagonal symmetry as predicted by these models. And if so, how far away are they from perfect hexagonal symmetry.

1.2 Goal of the thesis

This master thesis investigates the theoretical prediction of the formation of gaps of bare soil or spots of vegetation according to a hexagonal lattice. Spatial point pattern analysis provides methods for exploring and analysing spatial structures. Spatial descriptive measures give primary insights into the behaviour of point patterns, and give further rise to the development of tests to verify any hypothesised point process model. Initial interest is in testing Complete Spatial Randomness against the alternative hypothesis of regularity. This is done by comparing some of the descriptive measures for the observed point pattern to Monte Carlo simulations of a homogeneous Poisson point process. In case of rejection of the null hypothesis in favour of the alternative, further analyses are conducted with respect to the expected hexagonal symmetry. However, since perfect hexagonality is never achieved in reality, a sampling mechanism for near-hexagonal symmetry is developed. Simulations from such a sampling mechanism should represent point patterns that arose from a perfect hexagonal lattice by adding a certain amount of noise. These simulations can then be used to test the hypothesis of near-hexagonal symmetry and to derive useful parameters that can serve as deviation indices from perfect hexagonality.

1.3 Approach and outline of the thesis

Chapter 2 will elaborate on the scientific and statistical methods used. First, the general methodology of spatial point processes is outlined. Further, several summary characteristics are explained, followed by some edge correcting techniques. Also, the properties of the random, nearly hexagonal and some other nearly regular point processes are explained. After elaborating on the estimation of parameters and hypothesis testing, the chapter ends with an overview of the software used to perform the analyses. The data under research and the results of the analyses are presented in Chapter 3. This master thesis ends with the main conclusions, followed by a discussion of the conducted analyses and further recommendations in Chapter 4.

Chapter 2

Methods on Spatial Point Processes

2.1 Basic concepts

A *spatial point process* is a random collection of points falling in some d-dimensional space (most often 2- or 3-dimensional). These points represent the locations of an event in space. In practice, one often has only a single realisation of such a spatial point process, which is called a *spatial point pattern*. Spatial point patterns are defined within a bounded observation window, which can be a rectangle or any polygon. Most often the observed point pattern is only a sample of a pattern that is much larger. Examples of spatial point patterns are positions of trees or plants (ecology), epicentres of earthquakes (seismology), locations of stars (astronomy), home locations of infected individuals (epidemiology) ... . The goal of point process statistics is to analyse the geometrical structure of these point patterns, either by describing the geometrical properties of the pattern or by defining a suitable point process model for the pattern. These models try to describe the mechanism behind the generation of the observed point patterns.
Two main assumptions are made throughout this report: stationarity and isotropy. A *stationary* point process is a point process that is invariant to translations in the d-dimensional space, i.e. any relationship between two points depends only on the points' relative positions, not on the point locations. A point process is called *isotropic* if it is invariant to rotations about the origin. A point process that is both stationary and isotropic is called *motion-invariant*.

2.2 Summary characteristics

Typically, main interest is in detecting whether a point pattern behaves randomly, since this would mean that no interactions exist between the points in the point pattern. This state is referred to as Complete Spatial Randomness (CSR) (see Section 2.4.1). However, more interestingly would be when the point pattern deviates from this random nature, either by exhibiting regularity among the points or by forming clusters of points. In order to obtain knowledge about the spatial arrangement of point patterns, summary characteristics that describe the geometrical properties of point patterns are needed. From these summary characteristics it is possible to not only obtain qualitative knowledge about the spatial structure of point patterns, but also to quantify them for specific point pair distances. The ones discussed here are applicable for stationary point patterns observed in a 2-dimensional space. Summary characteristics can be either numerical or functional. Numerical characteristics are single

numbers, while functional characteristics are usually defined in function of a distance r. In addition, summary characteristics can be defined for either points or locations. *Points* refer to the observed points in the point pattern, whereas *locations* refer to all possible points that could be generated by the point process in the observation window.

2.2.1 Intensity

The mean behaviour of a stationary point process is described by the *intensity* λ, also called *point density* and is defined according to

$$E[\#\text{ points in } B] = \lambda \text{ area}(B),$$

i.e. the expected number of points in any subset B of the observation window W is equal to the intensity λ times the area of the subset B. A standard unbiased estimator of the intensity can be calculated from the observation window W by

$$\hat{\lambda} = \frac{\#\text{ points in } W}{\text{area}(W)}. \tag{2.1}$$

Many other intensity estimators exist, some solving the issue of uncountable patterns or others that are adapted to some edge-corrected estimator of another summary characteristic. Since these will not be explicitly used here, the interested reader is referred to Illian et al. (2008).

2.2.2 Distributional indices

Distributional indices are numerical characteristics which describe the distribution of certain properties allocated to each point or location. These properties are referred to as marks, denoted by $m(x)$. This mark is calculated from a local neighbourhood of x, which is either determined by the k nearest neighbours or by a disc of radius r. Most indices are defined in function of the expected mark for a random point or location x, denoted by $E_x[m(x)]$. This expectation is estimated as the mean mark over all points or locations in the observation window W,

$$\frac{\sum_x m(x)}{\#\text{ points or locations in } W}. \tag{2.2}$$

When locations instead of points are considered, a random set of test locations are used in the estimation.

Aggregation or Clark-Evans index

The marks in the Clark-Evans index (Clark & Evans, 1954) are equal to the nearest neighbour distances. The index is defined as

$$CE = 2\sqrt{\lambda}E_x[d(x)] \tag{2.3}$$

where $E_x[d(x)]$ is the expected distance from a random point x in the point pattern to its nearest neighbour. The Clark-Evans index was originally developed to test for CSR. Therefore, the expected

nearest neighbour distance is standardised according to the nearest neighbour distance expected under CSR, which is equal to $1/(2\sqrt{\lambda})$. Therefore a CSR process is characterised by $CE = 1$.

Mean-direction index

The mean-direction index considers the vectors pointing from a random point x to its k nearest neighbours. These vectors are standardised to each have length 1. For a random point x in the point pattern, the mark is defined as the length of the sum of its unit vectors,

$$R_k(x) = |e_1(x) + e_2(x) + ... + e_k(x)|$$

for a fixed number of neighbours k. If two vectors are pointing in the exact opposite direction, they cancel out in the sum. The sum becomes maximal when all unit vectors would point in the same direction. The mean-direction index is simply the expectation of $R_k(x)$, denoted by $E_x[R_k(x)]$ (Corral-Rivas, 2006). The mean-direction index is useful in identifying regular patterns, since then each vector would match with a vector pointing in the exact opposite direction.

Degree of hexagonality

The degree of hexagonality aims at detecting a regular hexagonal lattice in the plain. Illian et al. (2008) defines the mark of a random point x in the point pattern by

$$H_6(x) = \sqrt{\left(1 + \sum_{j=2}^{6} \cos 6\beta_{xj}\right)^2 + \left(\sum_{j=2}^{6} \sin 6\beta_{xj}\right)^2}$$

where $i = \sqrt{-1}$ and the angles β_{xj} are the clockwise angles between a fixed reference unit vector $e_1(x)$ and all other unit vectors $e_j(x)$ $(j = 2, ..., 6)$. If the angles are integer multiples of 60°, then $6\beta_{xj}$ is equal to an integer multiple of 360°. In this case the sine equals 0 and the cosine equals 1, yielding $H_6(x) = 6$ in case of hexagonality. The degree of hexagonality is again defined in function of the expectation, $E_x[H_6(x)]/6$. This index takes the value 1 for a hexagonal lattice. However, since the index does not account for the distances to the nearest neighbours (which needs to be equal for hexagonality), other structures such as clustered patterns also take values for $E_x[H_6(x)]/6$ near 1.

Topological characteristics

Based on what is called the Voronoi tessellation, several useful characteristics can be defined. In general, tessellations divide the plane into non-overlapping polygons. The Voronoi tessellation plays an important role in spatial point pattern analysis. Define the nearest neighbour of a random point x in the plane by $n(x)$. The Voronoi tile $T(x)$ of a random point x in the point pattern is defined as

$$T(x) = \{\text{all locations } y \in W \text{ for which } n(y) = x\}.$$

The Voronoi tile $T(x)$ contains all locations in the observation window W that are closer to x than to any other point in the point pattern. Points within a Voronoi tile have a unique nearest neighbour in the point pattern, while points on the boundary of a Voronoi tile have two or more nearest neighbours

in the point pattern. Figure 2.1 shows the Voronoi tessellation of a CSR pattern.

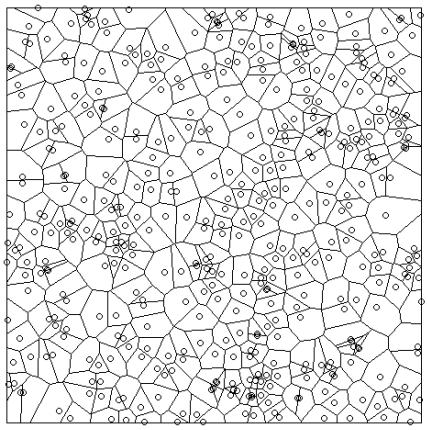

Figure 2.1: Voronoi tessellation.

Several marks can be defined to each point based on its Voronoi tile. Most commonly, these marks are the area $A(T(x))$, perimeter $P(T(x))$ and the number of sides/vertices $n(T(x))$ of the Voronoi tile. Useful characteristics are based on the mean and standard deviation of these marks. The number of sides/vertices for each tile provides a geometrical definition for the number of neighbours of each point in the point pattern.

In general, distributional indices are not the most informative summary characteristics in the presence of mapped point patterns. They are aggregated in the sense that they only consider summary statistics of the distribution. The distribution as a whole is not considered and other additional information such as range, standard deviation and mode are not always provided. These indices merely represent an easy way to get a quick first impression about the observed point pattern. Although these indices are of a certain valuability, other summary characteristics need to be considered to add to a thorough exploratory data analysis.

2.2.3 Functional characteristics

In contrast to the distributional indices, the functional summary characteristics are able to describe the full distributions that characterise a point pattern. The main advantage is that they provide knowledge on point interactions at different spatial scales.

Spherical contact distribution function or F-function

The spherical contact distribution function (also called the F-function) represents the probability that there is at least one point in the point pattern that is located within a distance r from a randomly chosen test location in the observation window W. This is equivalent to the probability that the distance between a randomly chosen test location and its nearest neighbour within the point pattern is less than r,

$$F(r) = P(d(x) \leq r) \quad \text{for} \quad r \geq 0,$$

with $d(x)$ equal the nearest neighbour distance for a randomly chosen test location x within the observation window W. In order to estimate $F(r)$, a random set of locations L within the window W is considered. The F-function can then be estimated for each distance r by

$$\hat{F}(r) = \frac{\sum_{x \in L} I(d(x) \leq r)}{\#\text{ locations in } L}, \tag{2.4}$$

i.e. the number of locations in the random set L which satisfy $d(x) \leq r$ (for which the indicator function $I(d(x) \leq r)$ equals 1) divided by the total number of locations in L.

Morphological functions

Based on the spherical contact distribution function, three other important morphological functions can be defined. They all relate to the morphological properties of the region defined by the Minkowski addition of the point pattern with a disc of radius r (see Fig. 2.2). This Minkowski region M_r consists of all locations that are within a distance r from an observed point in the pattern. These locations are illustrated in Fig. 2.2 by the grey area.

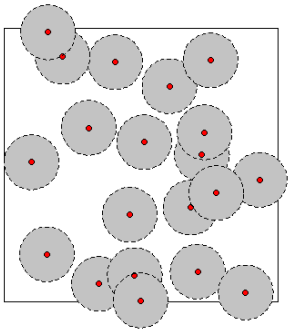

Figure 2.2: Minkowski addition.

The F-function can also be interpreted as the fraction of the window W which is covered by the Minkowski region, since this fraction equals the probability for a random test location to be within a distance r from a point in the point pattern. The latter is exactly the definition of the F-function. Also the fraction of the boundary length of the Minkowski region within W can be interpreted as the probability for a random test location to be at exactly a distance r from a point in the point pattern, which is nothing less than the density function of $F(r)$. Both functions are normalised by the area or boundary length fraction for non-overlapping discs, which equals $\lambda\pi r^2$ and $2\lambda\pi r$ respectively. Denote the normalised area fraction by

$$a(r) = f(r)/(\lambda\pi r^2) \quad \text{for} \quad r \geq 0, \tag{2.5}$$

where $f(r)$ is the density function of $F(r)$ and denote the normalised boundary length fraction by

$$l(r) = F(r)/(2\lambda\pi r) \quad \text{for} \quad r \geq 0. \tag{2.6}$$

The third function is related to the Euler or connectivity number. The specific Euler number for the Minkowski region M_r is defined as

$$N(r) = \lim_{K \uparrow \mathbb{R}^2} \frac{\boldsymbol{E}\chi(M_r \cap K)}{\text{area}(K)} \quad \text{for} \quad r \geq 0$$

where $K \uparrow \mathbb{R}^2$ is a sequence of growing sets K. The Euler number $\chi(M_r \cap K)$ is equal to the number of components in the set $M_r \cap K$ minus the number of holes in the set $M_r \cap K$. This function is again normalised by the corresponding quantity for non-overlapping discs, which equals λ,

$$n(r) = N(r)/\lambda \quad \text{for} \quad r \geq 0.$$

All three functions are equal to 1 for $r = 0$. For increasing r, both $a(r)$ and $l(r)$ decrease monotonically to zero. Only $n(r)$ is not necessarily monotonic, and can take on negative values. Estimators are obtained by calculating the observed fractions of the area, boundary length and Euler number of the Minkowski region within the observation window W. Illian et al. (2008) provides the estimation software for these functions at Penttinen (2008).

Nearest neighbour distance distribution function or G-function

The nearest neighbour distance distribution function (also called the G-function) is quite similar to the F-function, except that a random point within the point pattern is considered instead of a random test location in W. Similarly, the G-function can be interpreted as the probability that there is at least one point in the point pattern that is located within a distance r from a randomly chosen point in the point pattern. Again, this is equivalent to the probability that the distance between a randomly chosen point in the point pattern and its nearest neighbour within the point pattern is less than r,

$$G(r) = P(d(x) \leq r) \quad \text{for} \quad r \geq 0,$$

where $d(x)$ equals the nearest neighbour distance for a randomly chosen point x in the point pattern. The naive estimator for $G(r)$ equals

$$\hat{G}(r) = \frac{\sum_x I(d(x) \leq r)}{\#\text{ points in } W}, \tag{2.7}$$

i.e. the number of points in the point pattern which satisfy $d(x) \leq r$ (for which the indicator function $I(d(x) \leq r)$ equals 1) divided by the total number of points in the observation window W. The G-function interpreted on its own can provide misleading conclusions. Consider for instance a point pattern consisting of isolated pairs of points with an interdistance of d. The observed G-function for this clustered point pattern cannot be distinguished from a regular lattice with grid cells of side length d. The G-function will conclude regularity in both cases. It is therefore advisable to always consider the intensity in addition to the G-function, since then it would be possible to differentiate between the two point patterns.

Ripley's K-function

All previous mentioned summary characteristics were of first-order, i.e. they refer to properties that relate to single points. Ripley's K-function is a second-order characteristic which refers to properties that relate to pairs of points. Many argue that second-order characteristics are more powerful to describe a point pattern. The distributional indices provide only aggregated information on point interactions that are confined to a local neighbourhood. Also, the G- and F-function give little or no information on points beyond the nearest neighbour. Although, second-order characteristics give more insights into the correlations among the points, previous discussed summary characteristics should still be considered as they explain other worthwhile aspects of a point pattern, that cannot be derived from second-order characteristics.
Ripley's K-function is defined as the expected number of other points located within a distance r from a random point in the point pattern divided by the intensity,

$$K(r) = E_x[\#\text{ points within a distance } r \text{ from } x]/\lambda \quad \text{for} \quad r \geq 0.$$

The estimator for the K-function can be written in function of the number of pairs of points in the point pattern that lie within a distance r from each other (for which the indicator function $I(d_{ij} \leq r)$ equals 1),

$$\hat{K}(r) = \frac{1}{\hat{\lambda}^2 \text{ area}(W)} \sum_i \sum_j I(d_{ij} \leq r), \tag{2.8}$$

where d_{ij} represents the distance between the ith and the jth point in the point pattern.

Remark. It should be noted that not one summary characteristic describes a point pattern completely. Each characteristic describes different aspects of the point pattern and therefore contains valuable information. Consequently, hypothesis tests based on these summary characteristics can only accept or reject the null hypothesis with respect to the described behaviour. A typical point pattern analysis investigates several summary characteristics in order to draw an overall conclusion about the point pattern.

2.3 Edge corrections

Since the observed point pattern is restricted to a sample of a possibly much larger pattern, summary characteristics as introduced in Section 2.2 suffer from edge effects. In the absence of extra points outside the observation window W, points near the boundary of W will introduce bias in the calculation of summary characteristics if no edge correction mechanisms are applied. The naive estimators in Section 2.2 are adjusted with weights in order to alleviate the bias. In what follows, the most commonly used edge corrections will be explained shortly. These involve *no edge correction*, the *border method*, the *nearest neighbour edge correction* and the *second-order edge corrections*.
If both the observation window and the number of points are large, no edge correction is necessary. The bias introduced as such will only be minor and therefore edge effects can be ignored.
First-order summary characteristics typically use only the few neighbours that are located within a

distance r from each point in the point pattern. Therefore, considering only those points located at least a distance r away from the border of the window corrects for the bias. In Fig. 2.3(a) only those points crossed in red would be considered in the estimation. This edge correction is called the border method. The same method is sometimes also referred to as minus or reduced sampling, explained by the fact that only those points within a subwindow of W are considered in the estimation. This method has however the disadvantage to discard many data points for large r.

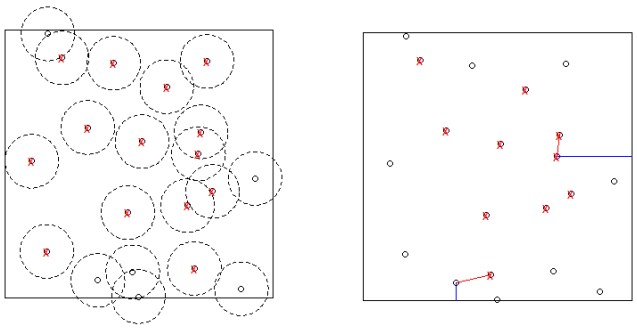

(a) Border method (b) Nearest neighbour method

Figure 2.3: First order edge corrections.

The nearest neighbour edge correction is an improvement on the border method since it determines for each point separately whether its nearest neighbours will be inside the window W. If the summary characteristic makes use of the k nearest neighbours, only those points for which the kth nearest neighbour distance (red in Fig. 2.3(b) for $k = 1$) is smaller than its distance to the boundary of the window (blue in Fig. 2.3(b) for $k = 1$) are considered in the estimation. In Fig. 2.3(b) these points are represented by red crosses. By this criterion large k-nearest neighbour distances are underrepresented and therefore the considered points are weighted by the inverse of the area of the subwindow constructed by reducing each boundary edge of W by the kth nearest neighbour distance. This weight is large for large kth nearest neighbour distances. For a square window, this area is simply $(l - 2 * k\text{th nearest neighbour distance})^2$ where l is the edge length of the window.

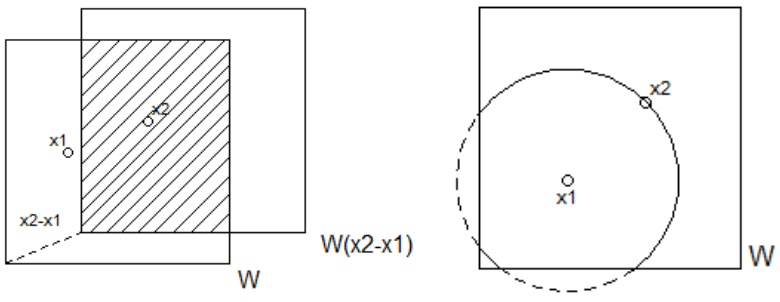

(a) Stationary edge correction (b) Isotropic edge correction

Figure 2.4: Second order edge corrections.

The border method and the nearest neighbour edge correction are primarily applied to first-order characteristics. Second-order characteristics will need other edge corrections in order to be unbiased. These characteristics typically involve all pairs of points and use their interpoint distances. The

stationary and isotropic edge corrections are constructed as such to give large weight to pairs with a large interpoint distance. The reason for which is the underestimation of the number of pairs with a large interpoint distance due to the bounded window. The stationary edge correction can be applied to all stationary point processes, whereas the isotropic edge correction can only be applied if the point process is isotropic in addition to the stationarity. The stationary or translational edge correction assigns the weight $1/\text{area}(W \cap W_{x_2-x_1})$ where $W_{x_2-x_1}$ represents the window W that has been translated according to the vector $x_2 - x_1$ (Fig. 2.4(a)). If the interpoint distance is large, the overlap will be small and therefore the weight will be large. The isotropic or rotational edge correction assigns the weight $1/w(x_1, x_2)$, which represents the boundary length in the window W of the circle with radius $\|x_1 - x_2\|$ and centre x_1 divided by the perimeter length of the circle, $2\pi\|x_1 - x_2\|$ (Fig. 2.4(b)). Again, if the interpoint distance is large, only a small proportion of the boundary will be inside the window, which corresponds to a large weight.
The edge-corrected estimators are constructed by weighting the summations in (2.2), (2.4), (2.7) and (2.8).

2.4 Point process models

This section introduces the point process models underlying the hypotheses of randomness and near-hexagonal symmetry. In addition, if the hypothesis of near-hexagonal symmetry would be rejected, it is worthwhile to investigate other near-regular symmetries.

2.4.1 Homogeneous Poisson point process

The Poisson point process plays a central role in point process statistics. When analysing a spatial point pattern, interest lies in the interaction that exist between the points, since they explain their spatial arrangement. When no such interactions exist, the pattern is said to exhibit *Complete Spatial Randomness*. The theoretical basis for patterns with this property is established by the homogeneous Poisson point process. Deviations from CSR can go both ways, towards a more clustered pattern or towards a more regular pattern. However, more complex models can be build based on combinations of these three types of patterns (regular, CSR, clustered).
Formally, a homogeneous Poisson point process is defined by two fundamental properties (Illian et al., 2008):

- The number of points of the point pattern in any bounded set B follows a Poisson distribution with mean λ area(B) for some constant λ.
- The number of points of the point pattern in k disjoint sets form k independent random variables, for arbitrary k.

The constant λ in the first property corresponds to the intensity as introduced in Section 2.2. The second property reflects the completely random behaviour of the points. Figure 2.5 shows an example of such a homogeneous Poisson point pattern.

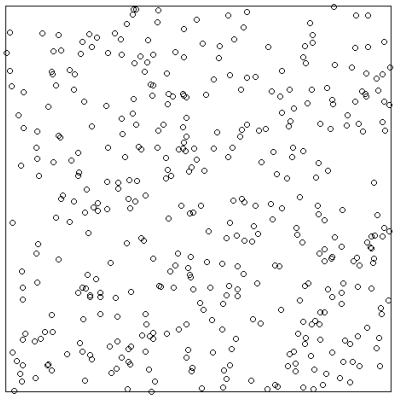

Figure 2.5: Homogeneous Poisson point pattern.

Based on the just mentioned properties, a point pattern from a homogeneous Poisson process is simulated as follows.

- Determine the total number of points N within the observation window W by drawing a random number from a Poisson distribution with mean λ area(W).
- Generate N times u and v coordinates from a uniform distribution on the intervals corresponding to the width and height of the observation window W.

For a homogeneous Poisson process, the analytical expressions of the summary characteristics are known. For instance, under a Poisson process the following relationship exists between the mean nearest neighbour distance δ and the intensity λ,

$$\delta^2 = \frac{1}{4\lambda}. \tag{2.9}$$

The Clark-Evans index was developed in such a way to take the value 1 for a Poisson process. Values larger than 1 correspond to regularity and values smaller than 1 to clustering. Although the mean direction index and the degree of hexagonality were originally developed to detect regularity or even more specific hexagonality, the theoretical values under a Poisson process are known and can be used, although maybe less powerful. The mean direction index takes on the values 1.575, 1.799, 2.007, 2.193 for $k = 3, 4, 5, 6$ respectively. Small values indicate a regular pattern, while large values refer to clustering. The degree of hexagonality takes the value $2.193/6 = 0.366$.
The topological indices for the Voronoi tessellation of a Poisson pattern follow the formulas in table Table 2.1.

Table 2.1: Theoretical topological indices for the Voronoi tessellation of a homogeneous Poisson process.

Characteristic	Mean	Variance	Standard deviation
Area	$\lambda\mu(A) = 1$	$\lambda^2\sigma^2(A) = 0.2802$	$\lambda\sigma(A) = 0.5293$
Perimeter	$\sqrt{\lambda}\mu(P) = 4$	$\lambda\sigma^2(P) = 0.9455$	$\sqrt{\lambda}\sigma(P) = 0.9724$
Vertices	$\mu(n) = 6$	$\sigma^2(n) = 1.7808$	$\sigma(n) = 1.3345$

The CSR F- and G-function coincide at the function $F_{CSR} = G_{CSR} = 1 - \exp(-\lambda\pi r^2)$. However, the direction of the deviation from this function has opposite meanings for the F- and G-function. If $\hat{F} > F_{CSR}$ or $\hat{G} < G_{CSR}$, the point process is more regular, while for $\hat{F} < F_P$ or $\hat{G} > G_P$ the point process is more clustered. Since these function coincide for the Poisson process, it is natural to define the J-function (van Lieshout & Baddeley, 1996) as

$$J(r) = \frac{1 - G(r)}{1 - F(r)} \quad \text{for} \quad r \geq 0, \quad \text{with} \quad F(r) < 1,$$

which equals 1 for a Poisson process. If $J(r) \leq 1$, then the process is more clustered, while the reverse is true for more regular processes. In essence, the J-function compares the environment of a random point to the environment of a random location. An estimator for $J(r)$ is constructed from estimators for $F(r)$ and $G(r)$.
The morphological functions take on the following expressions in case of a Poisson process

$$n_P(r) = (1 - \lambda\pi r^2)\exp(-\lambda\pi r^2),$$

$$l_P(r) = \exp(-\lambda\pi r^2),$$

$$a_P(r) = (1 - \exp(-\lambda\pi r^2))/(\lambda\pi r^2).$$

Regular patterns show a larger behaviour for small r, while for larger r they decrease rapidly and approach the Poisson process counterparts from below for increasing r. Clustered patterns show a smaller behaviour than the Poisson process counterparts for small r. The behaviour for larger r depends on the further spatial arrangement of the clusters.
The CSR K-function is equal to πr^2. More regular patterns correspond to smaller values, and more clustered patterns to larger values. When testing for CSR, the K-function is compared to a parabolic curve, which makes the interpretation somewhat more difficult. Therefore, one has defined the L-function

$$L(r) = \sqrt{\frac{K(r)}{\pi}} \quad \text{for} \quad r \geq 0$$

which is compared to the straight line r. This root transformation also has the tendency to stabilise the variance, which had an increasing behaviour for increasing r when estimating the K-function. Note that the L-function represents the same information as the K-function, only now with graphical and statistical advantages. For regular patterns, $L(r) < r$ and for clustered patterns, $L(r) > r$. Estimating the L-function is done by applying the root transformation on the estimator for K. The pair correlation function is another function derived from the K-function, but with an easier interpretation due to its non-cumulative nature. It is defined in function of the derivative of $K(r)$,

$$g(r) = \frac{K'(r)}{2\pi r}.$$

In case of a Poisson process, $g(r)$ equals 1. Larger values refer to a clustered process, and smaller values to a regular process. If a distance r_{corr} exists such that

$$g(r) = 1 \quad \text{for} \quad r \geq r_{corr},$$

then r_{corr} is called the range of correlation. No correlations are observed between points located more than a distance r_{corr} from each other. If a distance r_0 exists such that

$$g(r) = 0 \quad \text{for} \quad r \leq r_0,$$

then r_0 is called the hard-core distance or minimum interpoint distance. Estimators for the pair correlation function are based on a kernel smoothing method (Stoyan & Stoyan, 1994), which will not be discussed here.

2.4.2 Nearly hexagonal point process

In geometry, a regular hexagon is a polygon with 6 edges of the same length and 6 angles of 120° each. In a perfect hexagonal lattice each point has 6 neighbours which are located at the vertices of a regular hexagon that is centred at this point. Such a lattice is completely determined by the nearest neighbour distance. For a perfect hexagonal lattice, all Voronoi tiles are regular hexagons.
For a hexagonal lattice, the following relationship holds between the nearest neighbour distance δ and the intensity λ,

$$\delta^2 = \frac{2}{\sqrt{3}\lambda}. \tag{2.10}$$

Consequently, the Clark-Evans index equals $\sqrt{2/(\lambda\sqrt{3})}$. Therefore CE will reach his maximum value at $2\sqrt{2/\sqrt{3}} = 2.1491$. Naturally, the mean direction index with $k = 6$ equals 0 and the degree of hexagonality is equal to 1. The topological indices of the Voronoi tessellation for a hexagonal pattern are given by $\lambda\mu(A) = 1$, $\sqrt{\lambda}\mu(P) = \sqrt{24/\sqrt{3}} \approx 3.72$ and $\mu(n) = 6$. Due to its deterministic nature, all corresponding variances are equal to zero.
By using the geometrical properties of a hexagonal lattice, the expressions for the functional summary characteristics can be derived analytically. However, the expressions will not be given here, but will be illustrated in Chapter 3.

In nature, a perfect hexagonal lattice is difficult to find. However, patterns exist which seem to be almost perfectly hexagonal. A nearly hexagonal process can be simulated by allowing a deviation in some random direction for each point in the hexagonal lattice. One should however be aware that unobserved points located outside the window could end up inside the window by applying this deviation. Therefore, a larger initial window than the window of interest is considered for the hexagonal lattice. First a perfect hexagonal pattern is constructed in the enlarged window with a random positioning relative to the window. After adding the random deviations to the lattice of points, only those points that are located within the window of interest are considered further. The deviations are obtained by random sampling from a bivariate symmetric normal distribution with mean $(0, 0)$ and variance $\sigma^2 I_2$ (Fig. 2.6) with I_2 equal to the 2×2 identity matrix. Theoretically, the range of possible deviations is infinite according to the normal distribution, which makes it difficult to decide upon the size of the enlarged window. However a good choice would be to extend the window on each side by the critical value that corresponds to the 99th percentile of the corresponding normal distribution. Instead of defining the absolute deviation σ, it is more interesting to work with the

relative deviation β defined according to $\beta^2/\lambda = \sigma^2$. Since a large intensity corresponds to a small interpoint distance, a fixed relative deviation β_0 corresponds to a small absolute deviation. Small intensities correspond to large interpoint distances and therefore the absolute deviation for the same β_0 is larger. This approach will be useful when comparing different regular structures.

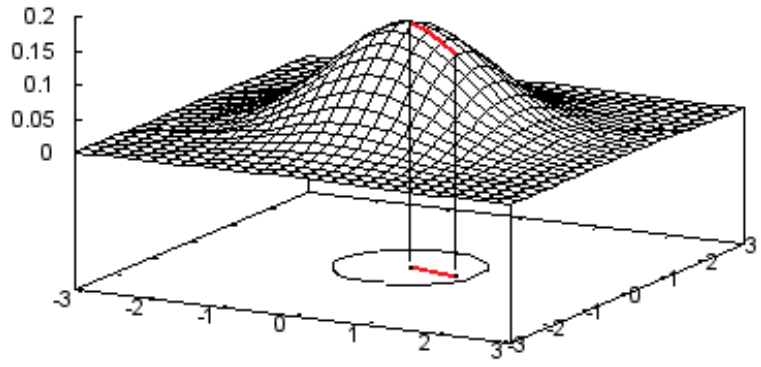

Figure 2.6: Random deviation according to a bivariate standard normal distribution $N((0,0), I_2)$.

Figure 2.7 shows a perfect hexagonal point pattern with three random examples of nearly hexagonal point patterns for $\beta = 0.1$, 0.2 and 0.5.

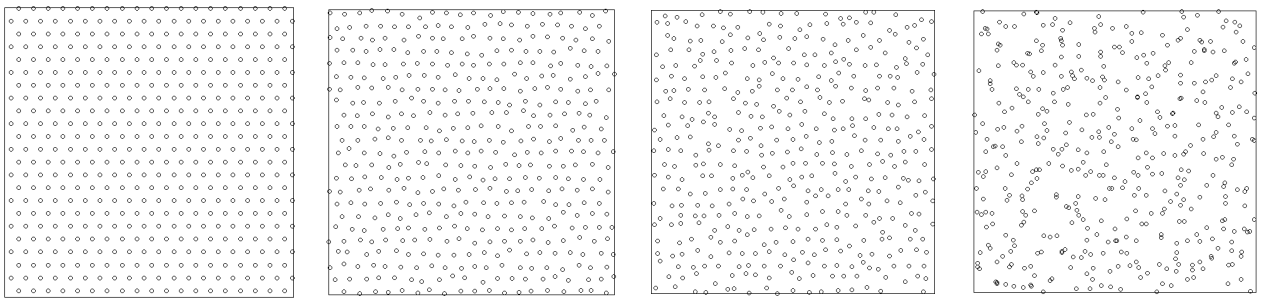

(a) $\beta = 0$ (b) $\beta = 0.1$ (c) $\beta = 0.2$ (d) $\beta = 0.5$

Figure 2.7: Nearly hexagonal point patterns.

2.4.3 Other nearly regular point processes

Nearly square point process

Geometrically, a regular square is a polygon with 4 edges of the same length and 4 angles of 90° each. In a perfect square lattice each point has 4 neighbours which are located at the vertices of a regular square that is centred at this point. For a perfect square lattice, all Voronoi tiles are regular squares. The summary characteristics for a square lattice are derived in a similar fashion as before. Here, the relationship between the nearest neighbour distance and the intensity becomes

$$\delta^2 = \frac{1}{\lambda}. \tag{2.11}$$

Consequently the Clark-Evans index is equal to 2 and the mean direction index with $k = 4$ is equal to 0. The topological indices become $\lambda\mu(A) = 1$, $\sqrt{\lambda}\mu(P) = 4$ and $\mu(n) = 4$ with zero variances.

Other summary characteristics will be illustrated in Chapter 3. Figure 2.8 shows a perfect square point patterns with three random examples of nearly square point patterns for $\beta = 0.1$, 0.2 and 0.5.

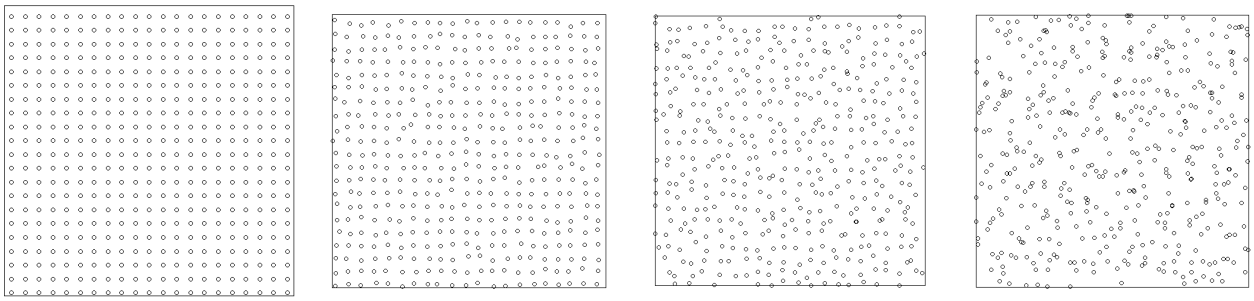

(a) $\beta = 0$ (b) $\beta = 0.1$ (c) $\beta = 0.2$ (d) $\beta = 0.5$

Figure 2.8: Nearly square point patterns.

Nearly triangular processes

A regular triangle is a polygon with 3 edges of the same length and 3 angles of 60° each. In a perfect triangular lattice each point has 3 neighbours which are located at the vertices of a regular triangle that is centred at this point. For a perfect triangular lattice, all Voronoi tiles are regular triangles. The relationship between the intensity and the nearest neighbour distance is defined as

$$\delta^2 = \frac{4}{3\sqrt{3}\lambda}. \tag{2.12}$$

Consequently the Clark-Evans index takes the value $4/\sqrt{3\sqrt{3}} = 1.7548$. The topological characteristics become $\lambda\mu(A) = 1$, $\sqrt{\lambda}\mu(P) = \sqrt{36/\sqrt{3}} \approx 4.56$ and $\mu(n) = 3$ with zero variances. Other summary characteristics will be illustrated in Chapter 3. Figure 2.8 shows a perfect triangular point pattern with three random examples of nearly triangular point patterns for $\beta = 0.1$, 0.2 and 0.5.

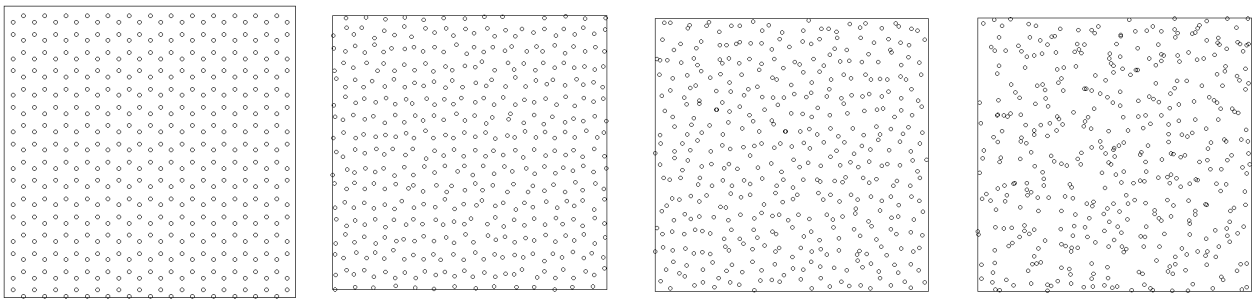

(a) $\beta = 0$ (b) $\beta = 0.1$ (c) $\beta = 0.2$ (d) $\beta = 0.5$

Figure 2.9: Nearly triangular point patterns.

Nearly rhomboidal processes

A rhomboidal lattice is closely related to both a hexagonal lattice as a square lattice, but allows for more flexibility in the pattern. In such a lattice, each point still has 6 neighbours as determined by the Voronoi tessellation, but these are not necessarily located around the point with the same distance. The lattice is constructed by reducing the 90° angle in a perfect square raster to an angle within the

range $(0° - 90°)$. The initial square raster unit changes into a rhomboidal raster unit. Choosing the angle equal to 60° or 90° corresponds respectively to the hexagonal and square lattice. Denote the angle by ϑ. Then all Voronoi tiles are hexagons with 2 opposite angles of $180° - \vartheta$ and 4 other angles of $90° - 0.5\vartheta$. When ϑ lies between 0° and 60° there are only 2 nearest neighbours located at the same distance. For ϑ between 60° and 90° there are 4 nearest neighbours located at the same distance. When ϑ is exactly equal to 60°, all 6 neighbours are located at the same distances, corresponding to the hexagonal pattern.
The relationship between the intensity and the nearest neighbour distance now becomes

$$\delta^2 = \frac{1}{2\lambda \sin(\vartheta/2)\cos(\vartheta/2)} \quad \text{for } 60° < \vartheta < 90° \tag{2.13}$$

and

$$\delta^2 = \frac{2\sin(\vartheta/2)}{\lambda \cos(\vartheta/2)} \quad \text{for } 0° < \vartheta < 60°. \tag{2.14}$$

Consequently the Clark-Evans index is equal to $\sqrt{2/(\sin(\vartheta/2)\cos(\vartheta/2))}$ for angles above 60° and to $\sqrt{8\sin(\vartheta/2)/\cos(\vartheta/2)}$ for angles below 60°. When the angle lies between 0° and 60°, the mean direction index with k =2 or 6 takes the value 0. When the angle lies between 60° and 90°, the mean direction index with k =4 or 6 equals 0. The behaviour of other summary characteristics is similar to the other regular patterns for $\vartheta > 40°$. Angles smaller than 40° lead to patterns that exhibit both clustering and regularity. These are not of interest in this context. Figure 2.10 shows a perfect rhomboidal point pattern (angle 70°) with three random examples of nearly rhomboidal point patterns for $\beta = 0.1$, 0.2 and 0.5.

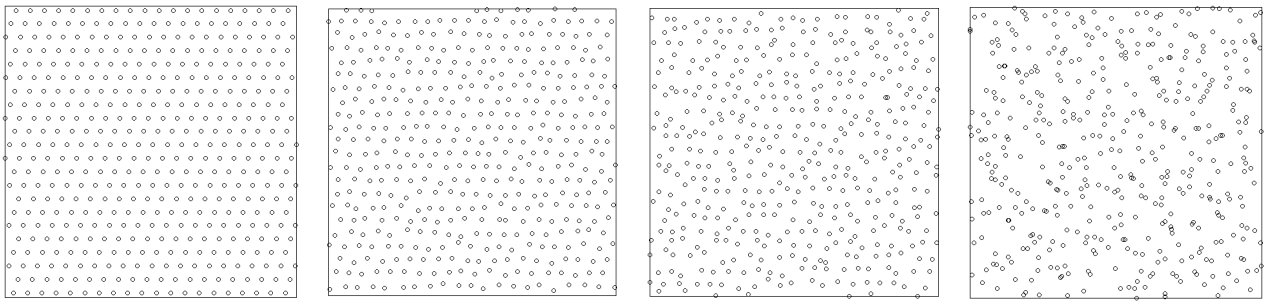

(a) $\beta = 0$ (b) $\beta = 0.1$ (c) $\beta = 0.2$ (d) $\beta = 0.5$

Figure 2.10: Nearly rhomboidal point patterns (70°).

In general, each nearly regular process has two main parameters, the intensity λ and the deviation β. The nearly rhomboidal point process has one additional parameter, the angle. For perfect regular patterns, the intensity has a one-to-one correspondence with the nearest neighbour distance δ through the relations in (2.10), (2.11), (2.12), (2.13) and (2.14). It is expected that the intensity will stay rather constant upon allowing a normal deviation in the perfect regular pattern. However, the nearest neighbour distance δ changes from a single value to a distribution of nearest neighbour distances. Also, the mean of this distribution is expected to differ from the initial nearest neighbour distance δ that defines the perfect regular pattern.

2.5 Parameter estimation in point process models

The parameters as estimated from the observed point pattern help in understanding the underlying process that constructed the observed point pattern. Typically, a point process model is characterised by only a few parameters, since too complex models are difficult to simulate and interpret. Therefore, the method often used in practice is the *method of moments*. This method tries to minimise a criterion with respect to the model parameters. Denote these model parameters collectively by $\boldsymbol{\theta}$. This criterion is equal to the difference between the theoretical form of a chosen summary characteristic S under the point process model of interest (denoted by $S_{\boldsymbol{\theta}}$) and this summary characteristic as estimated from the data $\hat{S}$. The estimator $\hat{\boldsymbol{\theta}}$ is the value $\boldsymbol{\theta}$ for which $\hat{S}$ and $S_{\boldsymbol{\theta}}$ are 'as close as possible'. A suitable summary characteristic is one that depends on $\boldsymbol{\theta}$ and is sensitive to variation in $\boldsymbol{\theta}$. It is either known analytically or can be easily derived from simulations. Model parameters that are among the summary characteristics explained in Section 2.2, can be estimated directly from the point pattern. For example, when the intensity λ is a model parameter, the estimator is simply $\hat{\lambda}$ as in (2.1), which is consistent with the method of moments. When the model parameter cannot be directly estimated from the data as such, one uses functional summary characteristics through the *minimum contrast method*. Basically,

$$\int_{s_1}^{s_2} |\hat{S}(r) - S_{\boldsymbol{\theta}}(r)|^p dr \tag{2.15}$$

is minimised with respect to $\boldsymbol{\theta}$. The parameters p, s_1, s_2 and the summary characteristic $S(r)$ can be chosen arbitrarily, but common practice is to use $p = 2$, $s_1 = 0$, $s_2 = s$ with s a suitable maximum distance. Typical choices for $S(r)$ are the L- or F-function. Many proposals about the choice for the maximum distance s have been made. Large distances r are often not bounded within the window W and there $S(r)$ cannot be estimated or only with large variance. Diggle (2003) suggests that s should not be bigger than $0.25l$ where l is the side length in case of a square window. In practice, the integral in (2.15) is replaced by a sum

$$\sum_{i=0}^{k} |\hat{S}(z_i) - S_{\boldsymbol{\theta}}(z_i)|^p \tag{2.16}$$

where $z_0 = s_1$, $z_i = s_1 + i\gamma$ $(i = 1, ..., k-1)$ and $z_k = s_2$ with $\gamma = (s_2 - s_1)/k$. As a function of $\boldsymbol{\theta}$, the expression in (2.16) can contain many local minima. Therefore, it is not recommended to use a automated optimisation algorithm, since then the global minimum will be missed. Instead, one often uses a grid search on the parameters.

For a Poisson process, the theoretical function $S_{\hat{\boldsymbol{\theta}}}(r)$ is often known, but for many other point process models no analytical expressions exist or are difficult to derive. These can however be estimated from the pointwise average of the summary characteristic coming from simulations from the point process model with fixed parameters $\boldsymbol{\theta}$. However, many simulations are needed to obtain a valid approximation of the theoretical function. Here, 'valid' is used in the context that enough simulations need to be conducted as to obtain the same estimates as would be obtained when the theoretical function was known exactly. The number of simulations needed is strongly connected to the precision by which one wishes to estimate the parameters. The higher the precision, the more simulations are necessary.

2.6 Hypothesis testing

Comparing the observed summary characteristic to the theoretical summary characteristic as expected under the null hypothesis does not provide any sense of variability. Therefore, when formally testing hypotheses, one typically uses Monte Carlo simulations. These simulations represent realisations of the point process model underlying the null hypothesis. As such, it is possible to define which deviations from the theoretical summary characteristic are small enough to be able to accept the null hypothesis.

Based on numerical summary characteristics

Denote the estimate of some numerical summary characteristic M by $\hat{M}$. A two-sided null hypothesis is rejected with significance level α if

$$\hat{M} > M_{\alpha/2} \quad \text{or} \quad \hat{M} < M_{1-\alpha/2}.$$

The critical values $M_{\alpha/2}$ and $M_{1-\alpha/2}$ can be derived through simulations of the underlying point process model. Denote by $\hat{M}_l$ the estimate of M for the lth simulated point pattern ($l = 1, ..., k$). Then, either the observed two-sided p-value can be calculated as

$$\hat{p} = \frac{1 + \sum_{l=1}^{k} I(\hat{M}_l > \hat{M})}{k+1}$$

or the critical values corresponding to significance level α can be derived by taking the $(\alpha/2)k$th highest and lowest value in the ordered sequence of $\hat{M}_l$.
When the null hypothesis is CSR, one-sided hypotheses can be tested with as alternative either clustering or regularity. The CSR hypothesis is then rejected if $\hat{M} < M_{1-\alpha}$ or $\hat{M} > M_{\alpha}$ in favour of the alternatives clustering or regularity depending on the definition of the summary characteristic. Here, M_{α} and $M_{1-\alpha}$ are respectively the αkth highest and lowest values in the ordered sequence of $\hat{M}_l$.

Based on functional summary characteristics

A hypothesis test based on a functional summary characteristic can follow two main approaches: an envelope test or a deviation test. The envelope test is based on k simulated point patterns ($l = 1, ..., k$) from the point process model underlying the null hypothesis. The upper and lower limits of the α-envelope of the summary characteristic $S(r)$ can be derived by taking the $(\alpha/2)k$ lowest and $(\alpha/2)k$ highest value of the sorted $\hat{S}_l(r)$ ($l = 1, ..., k$) for each r. The null hypothesis is accepted if the observed summary characteristic $\hat{S}(r)$ lies within this envelope for each r, otherwise it is rejected. For a fixed r, the error probability for a two-sided test equals $(\alpha k)/(k+1)$. However, this error probability cannot become smaller than $1/(k+1)$, since this would correspond to the pointwise minimum and maximum of $\hat{S}_l(r)$. In literature, choices for k satisfying $\alpha k \geq 5$ are recommended (Illian et al., 2008). However if all r are considered simultaneously, the true error probability will be larger than α. Although the envelope test has a pointwise interpretation, it is still a popular method that is used as a visual inspection to test hypotheses.

The deviation test provides a more formal and simultaneous hypothesis test. The deviation test is based on the same integral as in (2.15). The null hypothesis is rejected if

$$\hat{\Delta} = \int_0^s |\hat{S}(r) - S_{\hat{\boldsymbol{\theta}}}(r)|^p dr \geq \Delta_\alpha$$

where $S_{\hat{\boldsymbol{\theta}}}(r)$ is the theoretical summary characteristic for the point process model underlying the null hypothesis with estimated parameter $\hat{\boldsymbol{\theta}}$, and $\hat{S}(r)$ is the estimated summary characteristics for the observed point pattern. The critical value Δ_α can be derived from simulated point patterns from the point process model underlying the null hypothesis. Therefore, define

$$\hat{\Delta}_l = \int_0^s |\hat{S}_l(r) - S_{\hat{\boldsymbol{\theta}}}(r)|^p dr$$

where $\hat{S}_l(r)$ is the estimated summary characteristic for the lth simulated point pattern. In the same manner as in (2.16) the integrals are replaced by a sum. Now the observed p-value and critical value Δ_α can be calculated from the ordered sequence $\hat{\Delta}_l$ in the same way as for the numerical summary characteristics.

The most commonly used functional summary characteristics to test hypotheses are the F-function, the G-function and the L-function. The pair correlation function can also be used in the envelope test, but is not recommended for the deviation test. It is important to note that the envelope or deviation test should be based on a different summary characteristic than the one used for estimation. A test result based on the same summary characteristic as the one used for estimation is expected to be too optimistic.

2.7 Software

The software R 2.13.0 was used to define and explore point patterns, to estimate summary characteristics, to fit point process models and to test hypotheses. The main package used was 'spatstat' which provides several functions for the basics of point pattern analysis. Other more complex algorithms were programmed manually with these functions as basic elements.
As mentioned earlier Illian et al. (2008) provided a software package called Morph2D at Penttinen (2008) in order to estimate the morphological functions.

Chapter 3

Point Pattern Analysis

3.1 Point pattern under study

Figure 3.1(a) shows the satellite image of a vegetation pattern in the sub-Saharan Sahel, more specifically in Kenya with center coordinates 0°45'N 40°24'E. The image was obtained through Google Earth TM on January 22th, 2006 and stretches over a square area of 2530m × 2530m (6.4 square kilometres)). This flooded plain is vegetated with trees and shrubs and is characterised by spots of (almost) bare ground, shown in a brighter colour in Fig. 3.1(a). The points in the point pattern (Fig. 3.1(b)) represent the centres of the spots of bare ground. The scale unit is expressed in pixels and the pattern stretches over a square window of [0,863]×[0,863] pixels. The point pattern consists of 436 points and gives the impression of being a regular point pattern. The intensity of the observed point pattern as estimated by (2.1) was equal to 5.85×10^{-4} points per square pixel (6.81×10^{-5} points per square metre).

(a) Satellite image of periodic vegetation pattern in Kenya.

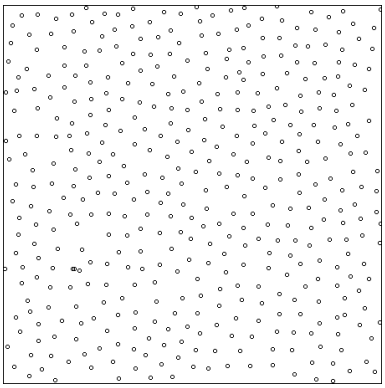

(b) Point pattern.

Figure 3.1: Data

3.2 Exploratory data analysis

Distributional indices

As recommended by Pommerening & Stoyan (2006), the nearest neighbour edge correction was used for the distributional indices. The nearest neighbour distribution is shown in Fig. 3.2. The minimum

nearest neighbour distance was equal to 3.16 pixels (37.09 metre). The largest observed distance was equal to 49.09 pixels (143.91 metre). The mean nearest neighbour distance was found to be 35.73 pixels (104.75 metre). Given the observed intensity, one would have expected a mean nearest neighbour distance of 20.67 pixels (60.60 metre) in case of a Poisson process. Larger values are an indication of more regular patterns. The maximum distance can only be obtained with a hexagonal structure and equals 44.43 pixels (130.25 metre). The expected mean nearest neighbour distances for a triangular or square structure are 36.28 pixels (106.36 metre) and 41.34 pixels (121.19 metre) respectively. For a rhomboidal structure with for example $\theta = 50°$ or $\theta = 70°$ the expected mean nearest neighbour distances are respectively 39.91 pixels (117.00 metre) and 42.64 pixels (124.48 metre). The observed mean nearest neighbour distance shows a deviation from the Poisson process towards a more regular structure. If the observed point pattern represents a deviation from a perfect regular structure, its mean nearest neighbour distance will not resemble the original nearest neighbour distance in the perfect regular structure. Therefore, based on this summary measure, one cannot decide on the most suitable nearly regular structure.

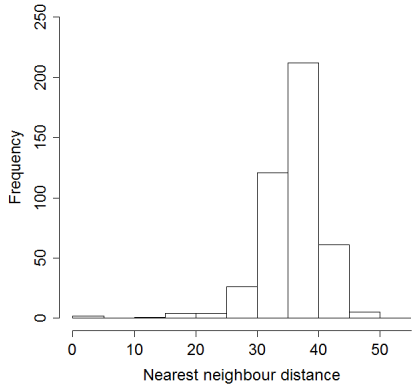

Figure 3.2: Observed nearest neighbour distribution.

The above findings are well summarized by the Clark-Evans index, which was equal to 1.729 for the observed point pattern. This value is larger than 1, as expected under CSR. This confirms the regularity seen in the point pattern. The observed value is also smaller than those expected under perfect hexagonal (2.149), square (2), triangular (1.755) or rhomboidal patterns (1.931 for $\vartheta = 50°$, 2.063 for $\vartheta = 70°$). The observed mean direction indices calculated over 4 and 6 neighbours is equal to 0.938 and 0.825 respectively. Both values are smaller than their CSR counterparts of 1.799 and 2.193 respectively. Both lie in the range of regular patterns, although the values still seem considerably larger than zero. The observed degree of hexagonality is equal to 0.439 which is slightly larger than its CSR counterpart value of 0.366. Again, the value seems to be considerably smaller than 1, as expected under hexagonality.

Lucarini (2008) reports on the behaviour of the mean and standard deviation of the Voronoi area, perimeter and number of vertices/sides in case of nearly hexagonal, square or triangular patterns. Their conclusions are compared with the observed results. Since this paper did not incorporate nearly rhomboidal point processes, they cannot be used here for comparison. The topological indices were based on those points for which their Voronoi tile does not touch the window boundary. The Voronoi distribution of the number of sides/neighbours is shown in Fig. 3.3.

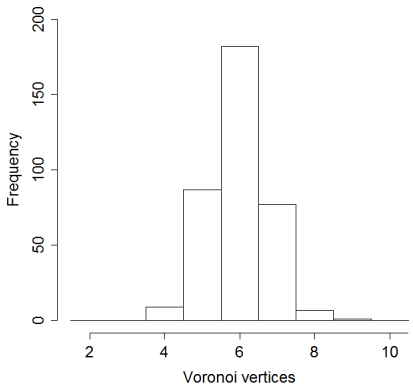

Figure 3.3: Observed Voronoi distribution of the number of sides/neighbours.

The mean number of neighbours was equal to 5.97. Its corresponding spread was characterised by a standard deviation of 0.81. Although a Poisson process also has a mean number of neighbours around 6, the observed standard deviation was less than the expected value of 1.33 under a Poisson process. The mean number of neighbours for a triangular or square pattern equals 3, respectively 4, but already upon the slightest deviation from these structures (as introduced in Section 2.4.2), the mean number of neighbours turns also to 6 with a spread starting from 0.93 for square patterns or 1.17 for triangular patterns which becomes larger for larger deviations. Deviations from hexagonality start off with a spread of zero which becomes larger for larger deviations. From $\beta > 0.5$ onwards the behaviour of the hexagonal, square and triangular patterns are indistinguishable. The observed value of 0.81 is unlikely to occur for nearly-triangular or nearly-square structures.

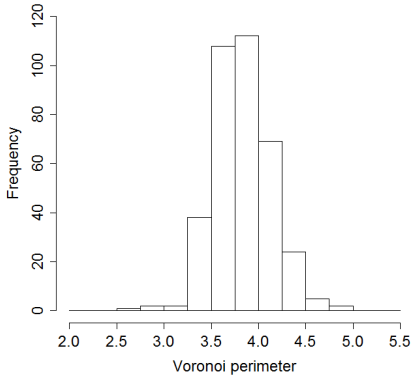

Figure 3.4: Observed Voronoi distribution of the perimeter.

The Voronoi distribution of the perimeter is shown in Fig. 3.4. The mean perimeter of the Voronoi tiles was equal to $3.83/\sqrt{\lambda}$ with a standard deviation of $0.30/\sqrt{\lambda}$. Both values deviate from what is expected under a Poisson process. Nearly hexagonal patterns can take mean perimeters between $3.72/\sqrt{\lambda}$ and $4.04/\sqrt{\lambda}$, nearly square patterns between $3.9/\sqrt{\lambda}$ and $4.04/\sqrt{\lambda}$ and nearly triangular patterns between $4/\sqrt{\lambda}$ and $4.56/\sqrt{\lambda}$. From $\beta > 0.6$ onwards, the three regular patterns become indistinguishable. Again the observed value is unlikely to occur for nearly-triangular or nearly-square patterns. The standard deviation of the perimeter shows very similar trends for all three nearly-regular patterns and is therefore not informative in this case.

The Voronoi distribution of the area is shown in Fig. 3.5. The mean area of the Voronoi tiles does not provide any information since it equals $1/\lambda$ for both a Poisson process as for the regular patterns. The observed standard deviation of the Voronoi area, $0.16/\lambda$, is however considerably smaller than its Poisson counterpart $0.53/\lambda$, providing evidence against CSR. Since the behaviour of the standard deviation for the nearly regular point processes behaves similarly, no further distinction between the patterns can be made based on this value.

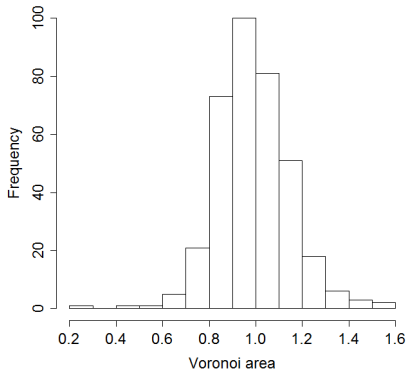

Figure 3.5: Observed Voronoi distribution of the area.

Functional summary characteristics

Figure 3.6 shows the functional summary characteristics for the observed pattern, together with the theoretical functions under CSR, hexagonal, square and triangular pattern with the same intensity as in the observed pattern. The rhomboidal functions are not shown here as not to overdue the figures. For angles between 40° and 90° they behave in a similar fashion as the other curves. The F- and G-function were corrected by the nearest neighbour edge correction, which is also most often used in practical applications. The edge-corrected J-function combined the nearest neighbour edge-corrected F- and G-function. Under the assumption of stationarity and isotropy, the isotropic edge-correction was used for the K-function, the L-function and the pair correlation function. Unbiased estimators for the morphological functions were obtained through minus sampling as stated by Illian et al. (2008).
Figures 3.6(a) and 3.6(b) show the F- and G-function. Deviations from CSR are in the direction of a regular pattern. The G-function shows a steep increase in the range of 25 to 45 pixels (73 to 132 metre), corresponding to a small spread around the mean nearest neighbour distance.
In comparing Figures 3.6(a) and 3.6(b), it is clear that $G(r) \leq F(r)$, which again is similar to the behaviour of a regular pattern. This conclusion is better visualised by the J-function in Fig. 3.6(c), which shows an overall upward deviation from the value 1 (CSR), towards regularity.
The three morphological functions are shown in Figures 3.6(d), 3.6(e) and 3.6(f). Again, the extensive period of close to 1 values represent the hard-core distance that is present in the observed data pattern. Regular patterns start off above their CSR counterparts and afterwards exhibit a steep decrease before they turn to zero. For moderate r both $l(r)$ and $n(r)$ take on values lower than their Poisson counterparts, where $n(r)$ typically takes on large negative values representing the number of holes contributed for by one point. All the observed functions lie in between the triangular and square functions.

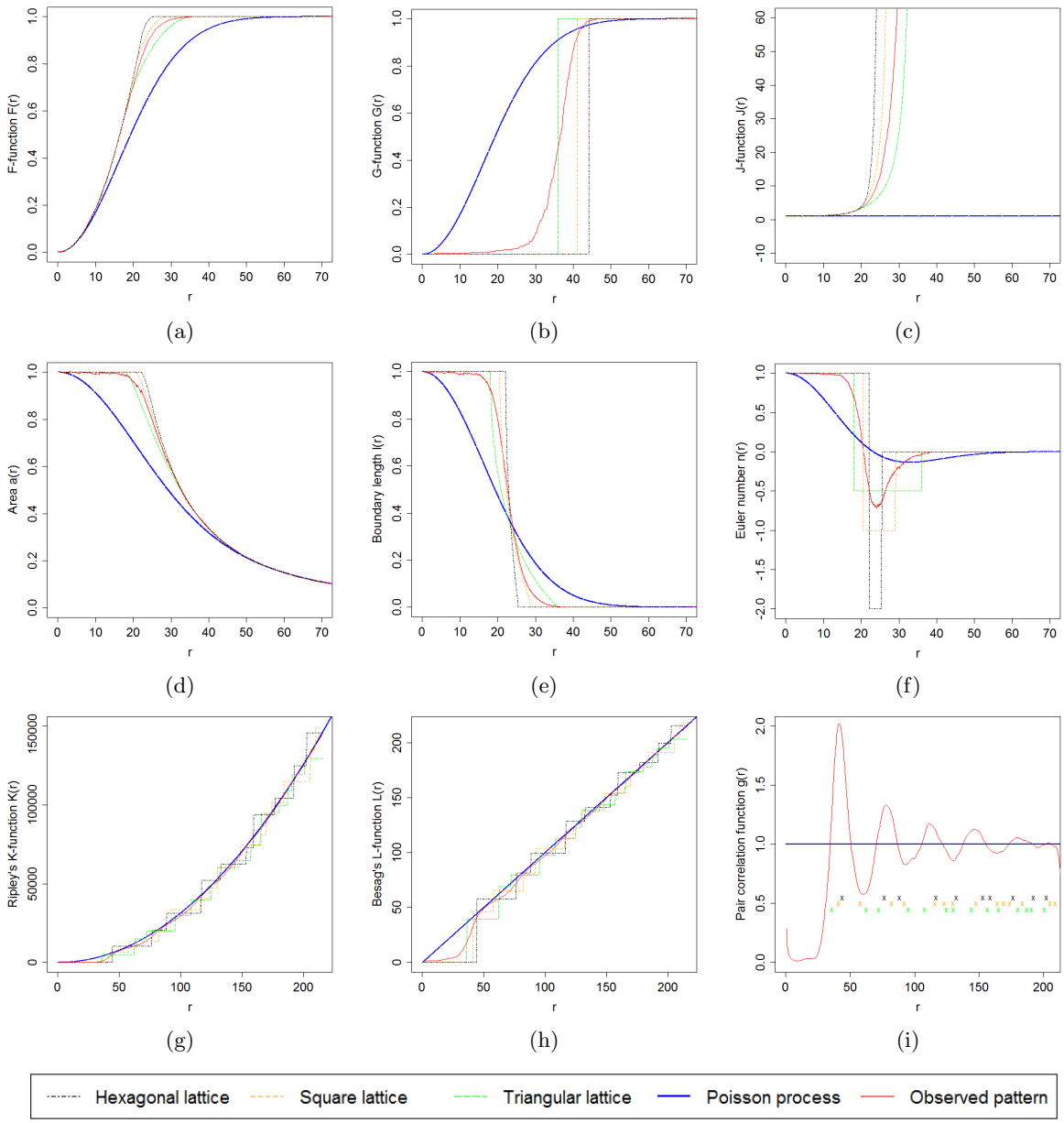

Figure 3.6: Observed functional summary characteristics compared to the theoretical summary characteristics under perfect regularity.

Figures 3.6(g) and 3.6(h) are able to show the long-range spatial interactions among the points in the point pattern. The observed point pattern shows the typical behaviour of a regular pattern. Initially the curve stays close to zero, corresponding to a hard-core distance, subsequently the curve will stay below its CSR counterpart for as long as the range of correlation stretches. Here, interactions play a role up to 150 pixels (440 metre), although the difference becomes rather small once past 80 pixels (235 metre).

Figure 3.6(i) shows the pair correlation function. Initially the curve shows a confusing behaviour concerning the hard-core distance. This behaviour is however due to a few single points that disturb the overall behaviour of the pattern and have their impact on the summary characteristics. One can conclude that there is a hard-core distance, but based on the pair correlation function it is difficult to determine its exact value. The pair correlation function is based on a smoothed kernel that is highly dependent on a smoothness parameter. Especially for small distances the pair correlation function

can be inaccurate. The subsequent behaviour of the pair correlation function is typical for a highly regular point pattern. The peaks correspond to the most frequent distances between the points and its nearest neighbours. In the near vicinity of a random point, points are located at a distance around 41 pixels (120 metre). Further on, additional peaks occur at 77.5, 111, 146 and 180 pixels (227, 325, 428 and 528 metre). The peak sequence shows a remarkable consistent regularity, since the peaks' interdistance are roughly consistent around 35 pixels (100 metre). The troughs correspond to the empty space in between the bands of points located at nearly the same distance from the typical point. The regular counterparts of the pair correlation function are shown by the crosses. Very high narrow peaks are expected at the location of the crosses. Many more peaks are expected in the case of a square or triangular lattice than that are observed.
In general, all functional summary characteristics lie in the region characterised by regular patterns. To assess whether the CSR hypothesis can be rejected in favour of regularity, formal tests are conducted in Section 3.3. For nearly regular patterns, almost all functions lie in between those corresponding to their perfect regular structure and the CSR counterpart. As the deviation from perfect regularity increases, the functions tend smoothly to the function corresponding to CSR. Therefore, it is very unlikely that the observed point pattern behaves like a nearly triangular point process. However, based on this exploratory data analysis no further conclusions can be drawn on the most suitable near- regular symmetry. Formal tests are applied in Section 3.4 and Section 3.5.

3.3 Complete spatial randomness

Estimation

The CSR hypothesis is characterised by the homogeneous Poisson point process with one model parameter, the intensity λ. As explained in Section 2.5 this intensity can be estimated directly from the observed point pattern by (2.1). The estimate for $\hat{\lambda}$ is equal to 5.85×10^{-4} points per square pixel. The following hypothesis tests are based on 1000 Monte Carlo simulations of a homogeneous Poisson point process with this estimate.

Tests based on distributional indices

The distributional indices provide a quick and easy way for CSR hypothesis testing. If the observed value is larger than the one-sided 5% critical value, the CSR hypothesis is rejected in favour of the regularity alternative at significance level 5%. The observed Clark-Evans index was equal to 1.729, which is larger than the 5% critical value 1.051. The mean direction index with 4 and 6 neighbours was also considered. Here, the observed value based on 4 neighbours was equal to 0.938, which is smaller than the 5% critical value 1.891. Based on 6 neighbours the observed value was equal to 0.825, which is again smaller than the 5% critical value 2.320. All tests reject the null hypothesis of CSR in favour of regularity.

Envelope tests

Figure 3.7 shows the 5%-envelopes of the different summary characteristics for 1000 simulations. The red curve shows the theoretical function in case of a Poisson process. None of the observed summary

characteristics lies completely within the envelopes. The morphological summary characteristics were not considered here due to computational difficulties in obtaining the area, boundary length or Euler number functions for 1000 simulated patterns.

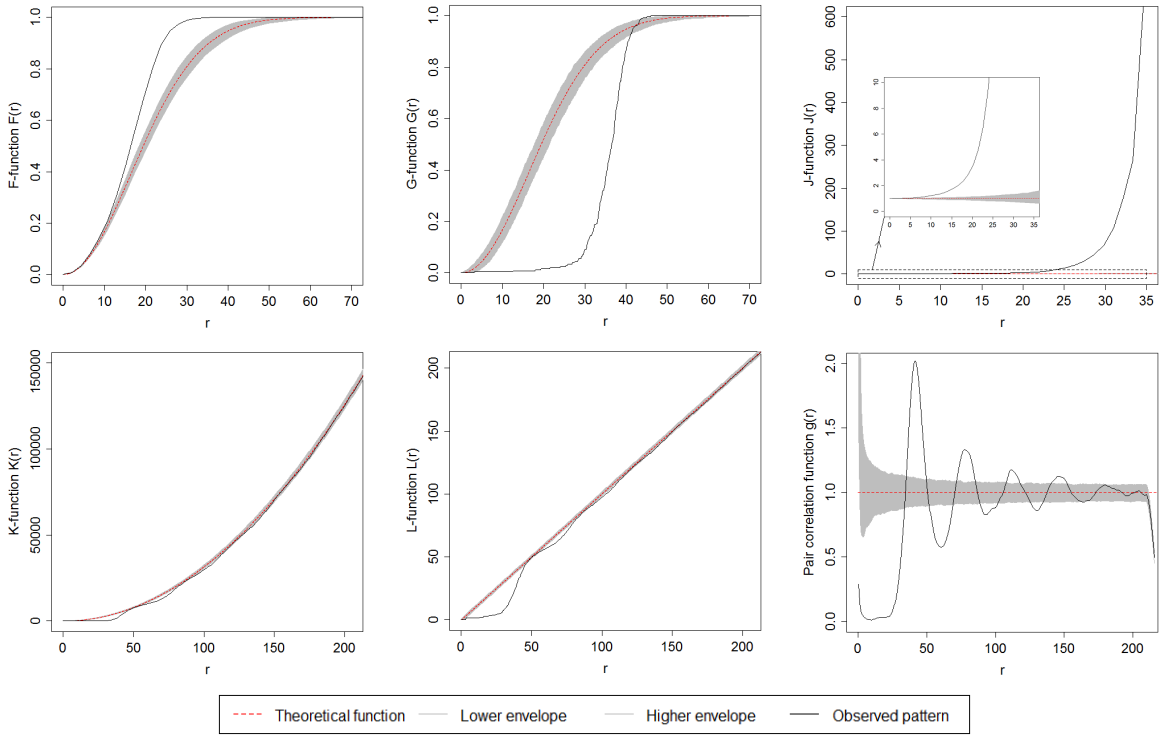

Figure 3.7: 5%-envelopes of the functional summary characteristics under Complete Spatial Randomness.

Deviation tests

The deviation test provides formal critical values for the CSR hypothesis. The maximal distance s in (2.16) was taken equal to $\lfloor 0.25 * l \rfloor = 215$ pixels (630 metre) for all functions except the J-functions since it is not defined for $F(r) = 1$. There s was set equal to 35 pixels (100 metre). The observed $\hat{\Delta}$ values together with the corresponding critical value Δ_α and p-values are given in Table 3.1.

Table 3.1: Deviation test for Complete Spatial Randomness hypothesis.

Characteristic	Observed $\hat{\Delta}$	Critical value Δ_α	P-value
F-function	0.3490	0.0060	*0.0010
G-function	53.0410	0.3250	*0.0010
J-function	501372.9000	0.8382	*0.0010
L-function	25 003.9700	1 181.0480	*0.0010

* $\hat{\Delta} > \max(\hat{\Delta}_l)$ $(l = 1, ..., 1000)$

The observed $\hat{\Delta}$ is larger than the critical value Δ_α for all summary characteristics. In general, it can be concluded that the observed point pattern rejects the CSR hypothesis and therefore does not originate from a homogeneous Poisson process.

3.4 Near-hexagonal symmetry

Estimation

A hexagonal point process model is determined by two parameters, the intensity λ and the deviation β. The intensity can be estimated directly from the observed pattern as before and is the same for all nearly regular processes, $\hat{\lambda} = 5.85 \times 10^{-4}$ points per square pixel. The deviation β is estimated through (2.16) with $S(r)$ taken equal to the L-function. The maximum distance used in the optimisation criterion (2.16) was again taken equal to $\lfloor 0.25l \rfloor = 215$ pixels (630 metre). Based on a 0.01 grid between 0 and 0.50 for β, 300 simulations seemed sufficient to safely assume that the pointwise average of these simulations was a good approximation of the true theoretical function. The deviation $\hat{\beta}$ was estimated at 0.15 for the nearly hexagonal point process.

Envelope and deviation tests

In testing the hypothesis of near-hexagonal symmetry, simulations from the underlying point process model need to account for the uncertainty around the obtained parameter estimates. The exact distributions describing this uncertainty are not known. Therefore, they need to be derived by a parametric bootstrap method. This method simulates independently m patterns from the point process model with parameters as estimated from the observed point pattern. Then the parameters $\boldsymbol{\theta}$ are estimated again for each simulated point pattern ($k = 1, ..., m$), denoted by $\hat{\boldsymbol{\theta}}_k$. If m is large enough, the $\hat{\boldsymbol{\theta}}_k$ are a valid approximation of the distribution of $\hat{\boldsymbol{\theta}}$. When simulating point patterns consistent with the null hypothesis of near-hexagonal symmetry, one first draws a random set of parameters from the distribution of $\hat{\boldsymbol{\theta}}$ and uses these fixed parameters to derive a nearly hexagonal point pattern as explained in Section 2.4.2. In addition, one could use the variance of the $\hat{\boldsymbol{\theta}}_k$ as an approximation to the variance of the estimator $\hat{\boldsymbol{\theta}}$. Also, the $\alpha/2$th and the $1 - \alpha/2$th quantiles can be used to derive a $(1 - \alpha)\%$ confidence interval. Due to heavy computation time, the method was conducted with $m = 50$ bootstrap patterns to derive the distribution of $\hat{\boldsymbol{\theta}}$. It should be noted that probably more bootstrap patterns are needed to obtain a valid approximation of the distribution of the estimated parameters. Therefore, the results should be interpreted with care. In the assumption that the 50 sets of bootstrap estimates are representative for their true distribution, 1000 simulations were used to derive the results for the envelope and deviation test.

The envelope tests are shown in Fig. 3.8. It is clear that all observed summary characteristics lie outside the 5%-envelopes expect for the F-function. This fact is also confirmed by the deviation test in Table 3.2. There, all tests are rejected at a 5% significance level except for the F-function.

Table 3.2: Deviation test for the near-hexagonal symmetry hypothesis.

Characteristic	Observed $\hat{\Delta}$	Critical value Δ_α	P-value
F-function	0.0013	0.0014	0.0689
G-function	1.7241	0.3770	*0.0010
L-function	1455.6290	285.4674	*0.0010

* $\hat{\Delta} > \max(\hat{\Delta}_l)$ $(l = 1, ..., 1000)$

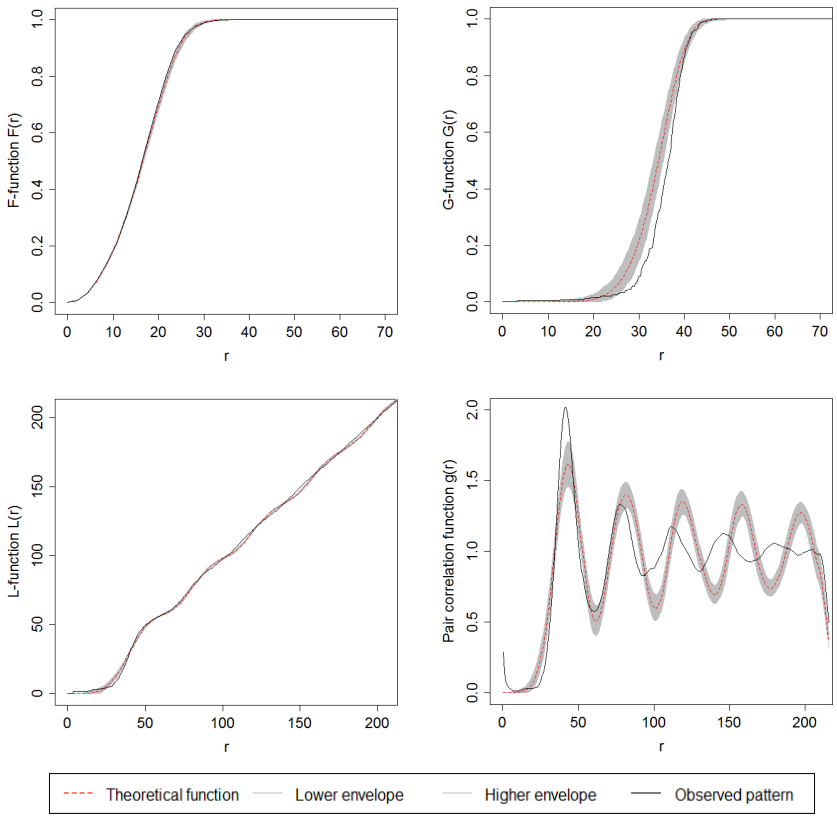

Figure 3.8: 5%-envelopes of the functional summary characteristics under near-hexagonal symmetry.

3.5 Other near-regular symmetries

Estimation

The same procedure as applied in Section 3.4 is used for the square, triangular and rhomboidal point process models. One has to account for the additional model parameter in the rhomboidal point process model, the angle ϑ. For that model, the minimum contrast method was based on an additional 1° grid between 40° and 90° for ϑ. The estimate for the intensity takes again the same value of 5.85×10^{-4}. The deviations $\hat{\beta}$ were estimated at 0.12, 0.15 and 0.16 respectively for the nearly rhomboidal ($\hat{\vartheta} = 52°$), square and triangular point processes.

Envelope and deviation tests

The envelope and deviation tests were conducted in the same manner as in Section 3.4. The envelope tests are shown in Figures 3.9, 3.10 and 3.11. It is clear that almost none of the observed summary characteristics lie completely within the 5%-envelopes. Only the F-function in case of the rhomboidal point process model seems to fit within the envelope for all r. When comparing all point process models, the point process model that resembles the data the closest, is the rhomboidal point process model, followed by the hexagonal point process model. The deviations from the square and triangular point process models are considerably larger.

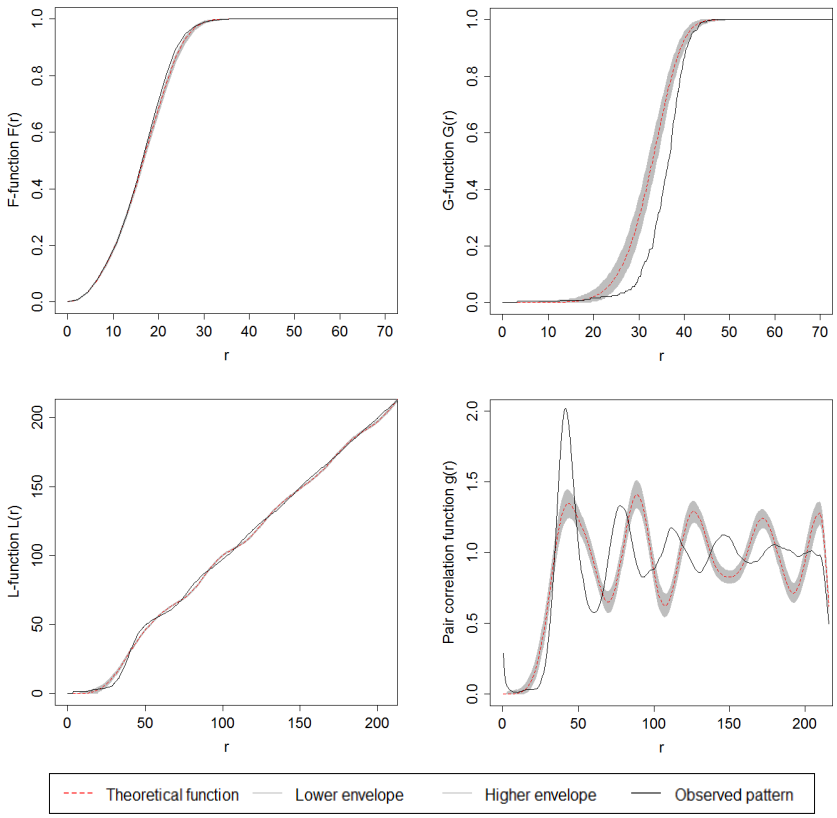

Figure 3.9: 5%-envelopes of the functional summary characteristics under near-square symmetry.

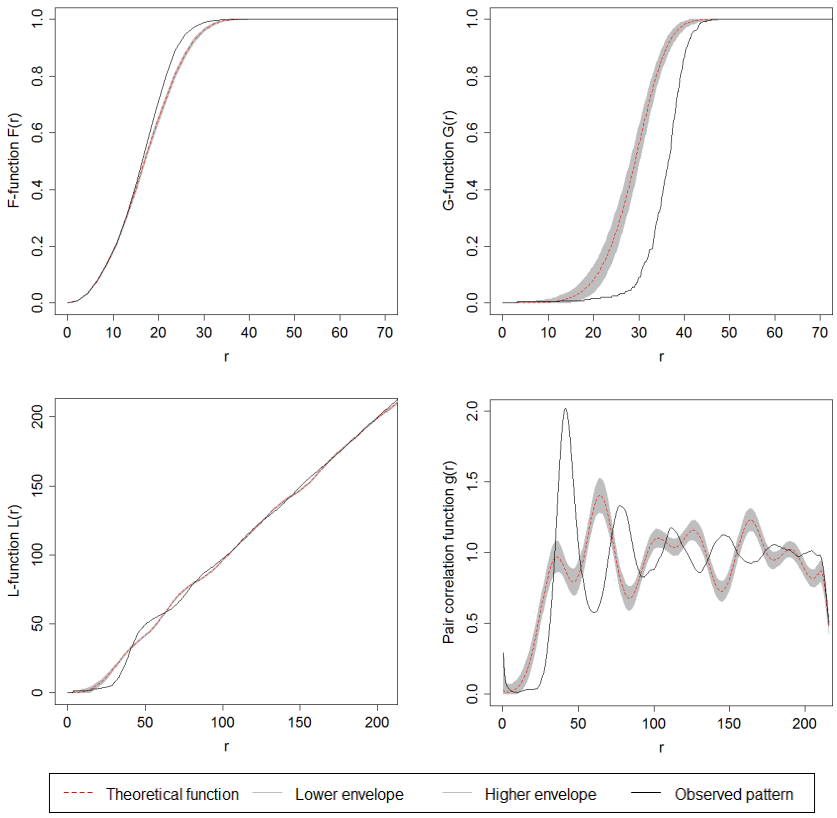

Figure 3.10: 5%-envelopes of the functional summary characteristics under near-triangular symmetry.

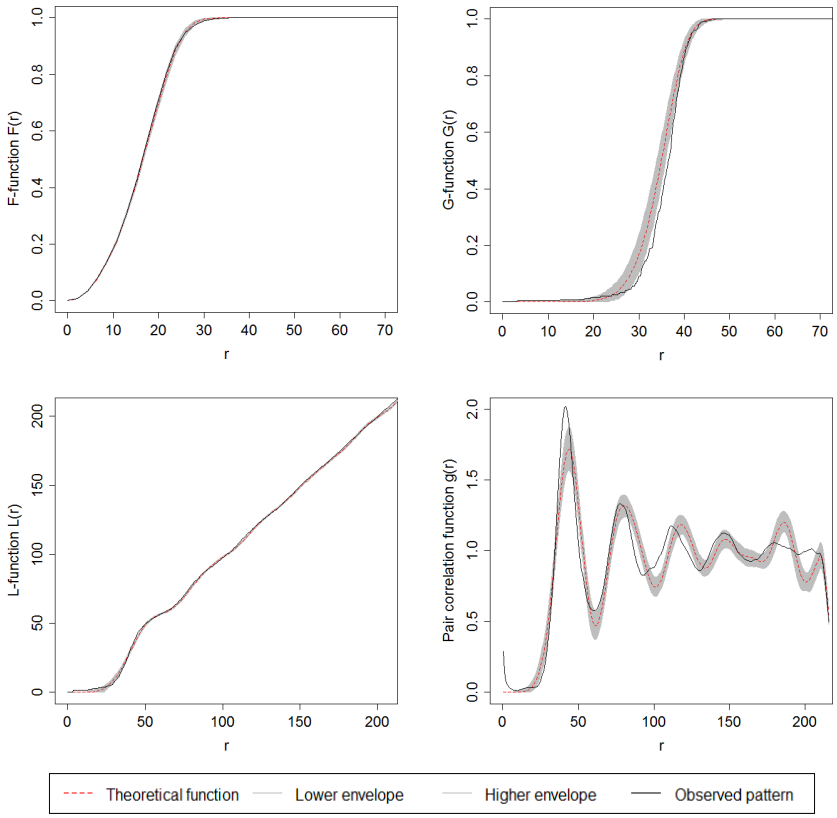

Figure 3.11: 5%-envelopes of the functional summary characteristics under near-rhomboidal (52°) symmetry.

The deviation tests in Table 3.3 confirms the conclusions from the envelope tests. There, all tests are rejected at a 5% significance level except for the rhomboidal F-function. Again, the rhomboidal point process model shows the smallest deviations $\hat{\Delta}$ for all functions. When comparing the observed G-function to the envelope in Fig. 3.11, the observed point pattern shows a slower increase for small distances r, i.e. there are less small nearest neighbour distances. This could imply that a different type of sampling mechanism that accounts explicitly for a hard-core distance between the points would fit the observed point pattern better.

Table 3.3: Deviation test for the near-regular symmetry hypotheses.

	Characteristic	Observed $\hat{\Delta}$	Critical value Δ_α	P-value
Nearly square pattern	F-function	0.0037	0.0011	*0.0010
	G-function	4.4095	0.2761	*0.0010
	L-function	2654.4870	237.9609	*0.0010
Nearly triangular pattern	F-function	0.0026	0.0007	*0.0010
	G-function	17.3016	0.3023	*0.0010
	L-function	6395.2360	212.9558	*0.0010
Nearly rhomboidal pattern	F-function	0.0007	0.0014	0.1768
	G-function	0.8609	0.3616	0.0030
	L-function	725.1517	250.4482	*0.0010

* $\hat{\Delta} > \max(\hat{\Delta}_l)$ $(l = 1, ..., 1000)$

Chapter 4

Concluding Remarks

4.1 Conclusion

For the Kenyan vegetation pattern under study, the null hypothesis of Complete Spatial Randomness was rejected in favour of a regular alternative. This conclusion was obtained unanimously by the distributional indices, the topological characteristics and the functional summary characteristics. The average intensity of the 2530 $\times$ 2530 square metre area was 1 point per 14680 square metre. The observed hard-core distance was equal to approximately 37 metres, whereas the average nearest neighbour distance was equal to 105 metre. Nearly regular point processes were developed by adding noise to the perfect regular grids. This noise was randomly drawn from a bivariate normal distribution with mean zero and some standard deviation. The exploratory data analysis showed that among the considered nearly regular point processes, the square and triangular point processes were very unlikely for the observed point pattern, whereas the rhomboidal and hexagonal point processes seemed more adequate. Estimation of the corresponding parameters by the minimum contrast method for the L-function yielded an intensity of 6.81 10^{-5} points per square metre and relative standard deviation parameters equal to 0.15, 0.12, 0.15 and 0.16 for respectively the nearly hexagonal, rhomboidal (52°), square and triangular point processes. These deviations corresponded to an absolute standard deviation of 18.2, 14.5, 18.2 and 19.4 metre. A formal acceptance of one of the near-regular symmetries was not established. However, since the observed summary characteristics differ only slightly from what would be expected for a near-rhomboidal point pattern, it can be concluded that this regular symmetry is the most likely for the observed data among the considered regular structures.

4.2 Discussion

There were several ways in which the conducted analysis was limited. A first practical issue was that the spatial point pattern analysis was a very computational intensive procedure. In order to obtain results within a feasible time frame, one had to pay off with precision. More specifically, in using 300 simulations to extract the theoretical summary characteristics for the nearly regular point processes, one could only obtain a relative standard deviation parameter β up to a precision of 0.01. For larger precisions, the L-function has to be known more accurately in order to obtain estimates that are not influenced by slight deviations in the L-function. In searching a grid of 5 possible β-values for estimation, already 1500 simulations were needed for which the L-function had to be estimated. This

drawback becomes even more pronounced when allowing for the uncertainty of the parameters in the hypotheses tests. For this reason, only 50 bootstrap patterns were considered in the derivation of the parameter distribution. These results need to be interpreted carefully, since probably more simulations are needed to obtain an adequate approximation of this distribution.
Throughout the analysis, many choices were made that were kept fixed. For instance, the maximum interaction range considered in the integral statistic was taken equal to 630 metre. Also the chosen summary characteristic for estimation was set to the L-function. One could perform a sensitivity analysis as to see whether different choices have a large influence on the results. This was however not conducted in this thesis for practical reasons. A full analysis lasted already 20 hours, making it very time consuming to consider multiple choices.

4.3 Recommendations

In general, a full sensitivity analysis should be conducted in order to see how sensitive the conclusions are to different choices. It is expected that the maximum interaction range or the choice of the summary characteristic for estimation will not show a major influence on the end conclusions. Increasing the number of simulations, both with respect to the bootstrap patterns as with respect to the approximations of the theoretical summary characteristic (here the L-function) could have a minor effect on the width of the envelopes. This would also make it possible to increase the precision of the grid search. Since the observed point pattern is already very close to the envelopes for near-rhomboidal symmetry, this could have an impact on the end conclusions.
However, it is expected that the very specific way in which the sampling mechanism for near-regular symmetry was developed (by means of the bivariate normal distribution) will have the largest influence on the end results. Based on the observed deviations from the envelopes, other sampling mechanisms that allow for a hard-core distance seem a good choice. Related to this remark, one could investigate a kind of hard-core point process where the neighbourhood of each point is completely random except for a hard-core distance. It is reasonable to explore such a model since recently self-organisation models have been developed that predict such a structure.
It is also recommended to analyse still other periodic vegetation patterns that exhibit gaps of bare ground, but also to consider vegetation patterns that consists of spots of vegetation. This way, one would be able to categorise all observed periodic vegetation patterns and even investigate whether the relative deviation from perfect regularity and the rhomboidal angle depend on other, maybe environmental, factors. Related to the initial research question, one could investigate under which conditions this angle is indeed equal to $60°$, i.e. the near-hexagonal symmetry.
Although for this observed point pattern, it was very reasonable to assume stationarity and isotropy, it could be that some form of heterogeneity disturbs the underlying near-regular symmetry and therefore the analysis is unable to verify this hypothesis. If the observed region is large enough, one could divide it into subregions that are expected to be homogeneous and to link the locally fitted point process models to variables that reflect this heterogeneity.

Bibliography

Clark, P. J., & Evans, F. C. (1954). Distance to nearest neighbour as a measure of spatial relationships in populations. *Journal of Ecology*, *35*, 445–453.

Clos-Arceduc, M. (1956). Etude sur photographies aériennes d'une formation végétale sahélienne: la brousse tigrée. *Bulletin de l'IFAN, Série A*, *18*(3), 677–684.

Corral-Rivas, J. J. (2006). *Models of Tree Growth and Spatial Structure for Multi-Species, Uneven-aged Forests in Durango (Mexico)*. Ph.D. thesis, University of Göttingen.

Deblauwe, V., Couteron, P., Lejeune, O., Bogaert, J., & Barbier, N. (2011). Environmental modulation of self-organized periodic vegetation patterns in sudan. *Ecography*. Doi: 10.1111/j.1600-0587.2010.06694.x.

Diggle, P. J. (2003). *Statistical Analysis of Spatial Point Processes (2nd edition)*. London: Arnold Publishers.

Illian, J., Penttinen, A., Stoyan, H., & Stoyan, D. (2008). *Statistical Analysis and Modelling of Spatial Point Patterns*. West Sussex, England: John Wiley & Sons.

Klausmeier, C. A. (1999). Regular and irregular patterns in semiarid vegetation. *Science*, *284*, 1826–1828.

Lefever, R., Barbier, N., Couteron, P., & Lejeune, O. (2009). Deeply gapped vegetaion patterns: On crown/root allometry, criticality and desertification. *Journal of Theoretical Biology*, *261*, 194–209.

Lefever, R., & Lejeune, O. (1997). On the origin of tiger bush. *Bulletin of Mathematical Biology*, *59*(2), 263–294.

Lucarini, V. (2008). From symmetry breaking to poisson point process in 2d voronoi tessellations: the generic nature of hexagons. *Journal of Statistical Physics*, *130*, 1047–1062.

Macfadyen, W. A. (1950a). Soil and vegetation in british somaliland. *Nature*, *165*, 121.

Macfadyen, W. A. (1950b). Vegetation pattersn in the semi-desert plains of british somaliland. *The Geographical Journal*, *116*, 199–211.

Meron, E., Gilad, E., von Hardenberg, J., Shachak, M., & Zarmi, Y. (2004). Vegetation patterns along a rainfall gradient. *Chaos Solitions and Fractals*, *19*, 367–376.

Penttinen, A. (2008). Software morph2d: Estimation of morphological functions.
URL `http://www.maths.jyu.fi/ penttine/ppstatistics`

Pommerening, A., & Stoyan, D. (2006). Edge-correction needs in estimating indices of spatial forest structure. *Canadian Journal of Forest Research*, *36*, 1723–1739.

Rietkerk, M., Boerlijst, M. C., van Langevelde, F., HilleRisLambers, R., van de Koppel, J., Kumar, L., Prins, H. H. T., & de Roos, A. M. (2002). Self-organization of vegetation in arid ecosystems. *American Naturalist*, *160*, 524–530.

Stoyan, D., & Stoyan, H. (1994). *Fractals, Random Shapes and Point Fields*. Chichester: Wiley and Sons.

Thiéry, J. M., d'Herbès, J.-M., & Valentin, C. (1995). A model simulating the genesis of banded vegetation patterns in niger. *Journal of Ecology*, *83*(3), 497–507.

van Lieshout, M. N. M., & Baddeley, A. J. (1996). A nonparametric measure of spatial interaction in point patterns. *Statistica Neerlandica*, *50*, 344–361.

Auteursrechtelijke overeenkomst

Ik/wij verlenen het wereldwijde auteursrecht voor de ingediende eindverhandeling:
Statistical analysis of the spatial symmetry of periodic vegetation patterns in semi-arid lands

Richting: **master of Statistics-Epidemiology & Public Health Methodology**
Jaar: **2011**

in alle mogelijke mediaformaten, - bestaande en in de toekomst te ontwikkelen - , aan de Universiteit Hasselt.

Niet tegenstaand deze toekenning van het auteursrecht aan de Universiteit Hasselt behoud ik als auteur het recht om de eindverhandeling, - in zijn geheel of gedeeltelijk -, vrij te reproduceren, (her)publiceren of distribueren zonder de toelating te moeten verkrijgen van de Universiteit Hasselt.

Ik bevestig dat de eindverhandeling mijn origineel werk is, en dat ik het recht heb om de rechten te verlenen die in deze overeenkomst worden beschreven. Ik verklaar tevens dat de eindverhandeling, naar mijn weten, het auteursrecht van anderen niet overtreedt.

Ik verklaar tevens dat ik voor het materiaal in de eindverhandeling dat beschermd wordt door het auteursrecht, de nodige toelatingen heb verkregen zodat ik deze ook aan de Universiteit Hasselt kan overdragen en dat dit duidelijk in de tekst en inhoud van de eindverhandeling werd genotificeerd.

Universiteit Hasselt zal mij als auteur(s) van de eindverhandeling identificeren en zal geen wijzigingen aanbrengen aan de eindverhandeling, uitgezonderd deze toegelaten door deze overeenkomst.

Voor akkoord,

Dupont, Vicky

Datum: **11/09/2011**